International Journal of Physical Modelling in Geotechnics
Volume 13 Issue 3

Water supply to a geotechnical centrifuge
Shepley and Bolton

International Journal of Physical Modelling in Geotechnics, 2013, **13**(3), 99–110
http://dx.doi.org/10.1680/ijpmg.13.00001
Paper 1300001
Received 03/01/2013 Accepted 14/06/2013
Keywords: centrifuge modelling/piles & piling

ice Institution of Civil Engineers
publishing

Water supply to a geotechnical centrifuge

Paul Shepley MEng
Lecturer, University of Sheffield, Department of Civil and Structural Engineering, Sheffield, UK

Malcolm D. Bolton FREng
Professor, Directory of the Schofield Centre, Cambridge University Engineering Department, Cambridge, UK

The supply of water to a centrifuge experiment has always been important. This paper details a new system which has been successfully commissioned for use on the geotechnical centrifuge at University of Cambridge. High water pressures and large flow rates were delivered to an experimental package, for the modelling of water injection-aided pile jacking. The practicalities of such a system are discussed in relation to existing alternatives, in addition to the precautions taken to ensure safe centrifuge operation. A method for calculating water pressures in the system away from instrumented locations is also proposed, using a linear relationship between energy per unit volume and the flow rate squared. Experimental data are presented to support these relationships.

Notation

A_{flow}	cross-sectional area of flow
a	loss factor
D	pipe diameter
ΔE	energy loss per unit volume
$\boldsymbol{g}$	gravitational acceleration
H_{loss}	pressure head loss
k	dimensionless loss factor for point losses
k_{s}	pipe roughness
L	pipe length
P_{p}	pump pressure
P_x	pressure at point x
Q	flow rate
R^2	linear regression
r_{w}	radial distance from beam centre to the phreatic surface
r_x	radial distance to point x
V_x	flow velocity at point x
λ	dimensionless loss factor for pipe losses
μ	fluid viscocity
ρ	fluid density
ω	angular velocity of centrifuge

1. Introduction

The geotechnical centrifuge is an important tool for modelling complex problems. Models often require either a water supply, or a means of moving water within the model, or possibly both. However, existing systems can be restrictive when attempting to model high flow rate problems.

To overcome this restriction, a new system was developed to supply high-pressure water to a centrifuge experiment at University of Cambridge. The system was designed to provide peak flow rates of 6 l/min, at pressures of up to 2 MPa. A flow rate control system was also incorporated into the design, capable of servo control.

This paper will address the commissioning of the new water supply system, the problems experienced and the solutions implemented. An analysis of the results will be presented that allows the robust calculation of pressures at points in the line remote from instrument locations. Finally, results will be presented from water injection-aided pile installations using the new water supply.

2. Background

2.1 Previous water supply methods

Centrifuge experiments requiring water supplies fall into two categories: open, and closed systems. Open systems are those where water is added to the experimental package from an outside source, such as by way of the centrifuge fluid slip rings. Open systems may be used to maintain a water table during a long centrifuge test: compensating for water loss through evaporation or accidental leakage. Typically, a standpipe is used to maintain a free water surface, expelling any excess water from the package into the centrifuge chamber, by over-topping a fixed drainage hole (Taylor, 1995). A device such as this prevents out-of-balance forces, which would otherwise increase if the water supply were maintained.

Closed systems are used in cases that require a volume of water to be moved within the package. Tunnel excavation or jetting of spudcan foundation problems (Gaudin *et al.*, 2011) make use of closed systems. Typically, an actuator-driven piston pump is used, where a piston is driven by a linear actuator and stepper motor. The actuator displacement directly controls the

flow rate exiting the piston, which provides the user with a high level of control. When using closed systems, the mass of the experiment package does not change, reducing the need for standpipes and similar apparatus.

However, piston systems have limitations. The total deliverable volume from a single piston stroke can restrict what is achievable in a single test. In addition, the system is limited by the capacity of the driving actuator. The actuator's ultimate load capacity limits the maximum fluid pressure, and its maximum speed limits the peak deliverable flow rate.

2.2 Design of a new water supply method

High flow rates and large pressures were desired in order appropriately to model the process of water injection-aided pile jacking in dense sands. In the field, pile jacking can be completed with supplementary water injection, using displacement pumps that generate maximum pressures between 5 and 10 MPa, and peak flow rates of 600 l/min (Tomlinson and Woodward, 2008).

A previous centrifuge model study of water injection-aided pile installation was described by Schneider *et al.* (2008). During testing, a piston pump was used to deliver a maximum pressure of 25 kPa at the pile head, two orders of magnitude lower than the pressure used at full scale. The flow rates sustained were also small, at 0·22 l/min. Additionally, owing to the capacity of the piston, water injection could only be used for a short period during pile installation. Each of these shortcomings is significant, but the lack of injection pressure is the most serious flaw for scaling between the centrifuge model and prototype conditions.

The aim of the tests detailed in this paper was to achieve model pressures comparable to those experienced on site. This accords with the principles of centrifuge modelling, which require similitude of the soil stresses and fluid pressures between the model and prototype scales (Ko, 1988).

The need for large injection pressures could not, however, be discounted. It was felt to be necessary to investigate whether water injection reduces pile driving loads through the reduction of effective stresses beneath the advancing pile. As base stresses are similar to cone penetration resistances, which can exceed 30 MPa at 10 m at prototype scale, it was decided that centrifuge injection pressures should be at least capable of exceeding 1 MPa. A high flow rate was anticipated in sands, and so a large water source was required. To achieve these flow conditions for an entire installation with a piston pump, a piston volume of 16 l and a maximum actuator force greater than 10 kN would have been necessary. Such large requirements were impractical, and a different supply solution had to be developed.

An alternative water supply was developed for use on the 10 m diameter Turner beam centrifuge at University of Cambridge. High pressures would be achieved by supplying water to the package through the fluid slip rings, and down the centrifuge arm. From a combination of pressurising the water before the slip rings, and the radial acceleration down the beam arm, maximum pressures exceeding 1 MPa at the package could be expected.

The pressure and flow rate provided to the experiment were monitored at the package, whereas a two-way solenoid valve was used to initiate water flow to the model pile. Flow rate control was achieved using a manual flow-control valve upstream of the centrifuge to avoid difficulty of operating a valve within the g-field.

2.3 Maintaining balance

High flow rates were predicted in sands by considering a steady flow Laplacian solution extending from a nozzle beneath an advancing pile to the sand and free water surface. This led to concerns about whether this excess water could be expelled from the centrifuge model without causing an out-of-balance problem. This had particular importance for the centrifuge at University of Cambridge, owing to the fixed mass counterweight (Schofield, 1980). Strict limits on the maximum change of mass of the experimental package are enforced, where 10 kg was the maximum allowable difference for short-term events.

To ensure the model stayed within this limit, a control system involving multiple pressure transducers was utilised. One transducer was used to monitor the water column height in the standpipe, ensuring drainage was taking place at all times. Further transducers were deployed to monitor any changes in the water surface in the sand body itself. The success of this system will be discussed in Section 6 of this paper.

2.4 Water injection-aided jacked piles

The motivation for the new water supply was to model jacked pile installations utilising supplementary water injection. The technique reduces the installation loads required for jacked pile installations (Tomlinson and Woodward, 2008). These loads can exceed 30 MPa on the pile base in hard ground, reducing the achievable piling rate or even causing pile refusal.

Only limited research has been completed on this process. Some field trials have been completed by the piling equipment manufacturer, Giken Seisakusho Ltd, but they remain unpublished. Typical injection operations used pump pressures greater than 2 MPa and flow rates between 100 and 350 l/min.

Centrifuge modelling of water jetted piles in silt has been undertaken by Schneider *et al.* (2008). However, the authors were unable to validate any mechanism governing the influence of water injection. The lack of other studies highlights the need for more work in order fully to investigate and verify the

governing mechanisms of water injection on pile installation, subsequent load capacity and possible disturbance to the surrounding ground.

3. System development

Three different water supply systems were trialled during the centrifuge test programme, and are presented in this paper. An iterative procedure was followed, basing improvements on the injection conditions achieved and the pile loads experienced using the previous system. All are shown schematically in Figure 1. A key is shown in the figure to clarify the different symbols used. Pressure locations are marked on the figure, denoted by P, with a subscript to indicate their location. Internal pipe diameters and lengths are annotated on appropriate lengths.

Typically, the pump pressure, P_p, was measured at the water supply to the slip rings. A flow-control valve was used to restrict the flow as necessary during the experiment, before passing fluid across the fluid slip rings. Pipe work along the beam arm was made in two lengths, 2 m of 15 mm internal diameter, and 2 m of a smaller, either 3·5 mm or 5·5 mm, diameter. Flow rate and pressure, P_2, were then monitored on the 'high pressure line', on board the experimental package.

The high pressure line is shown in Figure 2(a), and schematically in Figure 2(b). A turbine flow meter monitored the flow rate delivered to the package, and a pressure transducer measured the pressure in the line at this point. A two-way solenoid valve was used to activate the flow to the pile. A further pipe, 3·5 mm diameter, supplied water from the high pressure line to the pile. The pile had a smaller, 2·5 mm diameter, pipe running through the centre of the pile to supply water to the pile toe. This was terminated using a variety of nozzles of different geometries over the course of testing. It was important to assess the nozzle pressure throughout testing because that was the pressure to which the sand immediately in contact with the nozzle was exposed to.

System one connected the mains water supply, at a typical pressure of 200 kPa, directly to the centrifuge slip rings. Maximum pressures of 1·3 MPa were experienced at the package, under 60$\boldsymbol{g}$ acceleration, and peak flow rates of 3·2 l/min were achieved. However, fluctuations in the mains water supply pressure resulted in some variation in the pressure at the package. A manual flow tap was used in system one to restrict or cut off the flow supplied to the centrifuge.

System two replaced the direct link to the mains supply with a small impeller pump. The impeller pump system is shown in Figure 2(c) and schematically in Figure 2(d). The pump could deliver 700 kPa pressure with a flow rate up to 6 l/min. A pressure relief valve, set to 900 kPa, was used to prevent overloading of the slip rings. In addition, a remote controlled orifice valve was used to control the flow rate supplied to the slip rings as required.

System three used the same impeller pump as in system two. A larger bore pipe was utilised on the centrifuge, 5·5 mm in diameter rather than 3·5 mm, in order to reduce the pressure losses as water flowed down the beam arm. This had the benefit of a 10% increase in the maximum flow rate, reaching the maximum achievable 6 l/min.

4. Remote pressure calculation

The pressure at the pile nozzle was of most interest, whereas pressure could best be measured by a transducer off the high pressure line, far from the nozzle. Therefore, a relationship was required to determine the nozzle pressure, based on the monitored pressure at the high pressure line. This section describes the derivation of that relationship, and its validation using multiple data sets taken over the course of centrifuge modelling.

4.1 Energy loss

It is established that there is an energy loss associated with any variation to the cross-section for flow in a pipe. Losses arise over any significant pile length, or at certain locations, owing to constrictions, expansions and valves, for example.

All losses in the system can be shown as standard factors, to be multiplied by the flow rate squared, Q^2, where flow rate is given in cubic metres per second. The energy loss is typically represented by a head loss, H_{loss}, which is given in metres of pressure head; however, for this study the energy per unit volume, E, will be used. The energy per unit volume is linked to the flow rate by way of Equation 1

$$1. \quad \Delta E = \rho \boldsymbol{g} H_{loss} = a \times Q^2$$

where ρ is the density of the fluid in kilograms per cubic metres; $\boldsymbol{g}$ is the gravitational acceleration in metres per second squared; and a is the loss factor with units Ns/m^8. This formulation is a generalisation of typical expressions for pressure losses in pipe networks (White, 1998). The loss factor differs for point obstructions and pipe lengths according to the expressions

$$2. \quad \Delta E_{point} = \frac{\rho k}{2A_{flow}^2} \times Q^2 \text{ and } \Delta E_{pipe} = \frac{\rho \lambda L}{2DA_{flow}^2} \times Q^2$$

where A_{flow} is the cross-sectional area of the flow at the smallest section of interest in metres squared; D is the smallest diameter for the flow area in metres; L is the pipe length in metres; and k and λ are dimensionless factors used to find the loss, depending on the geometry of the problem. Each loss type will be considered in turn.

For point losses, the dimensionless factor k depends on the type of flow variation. Only one loss factor can be found

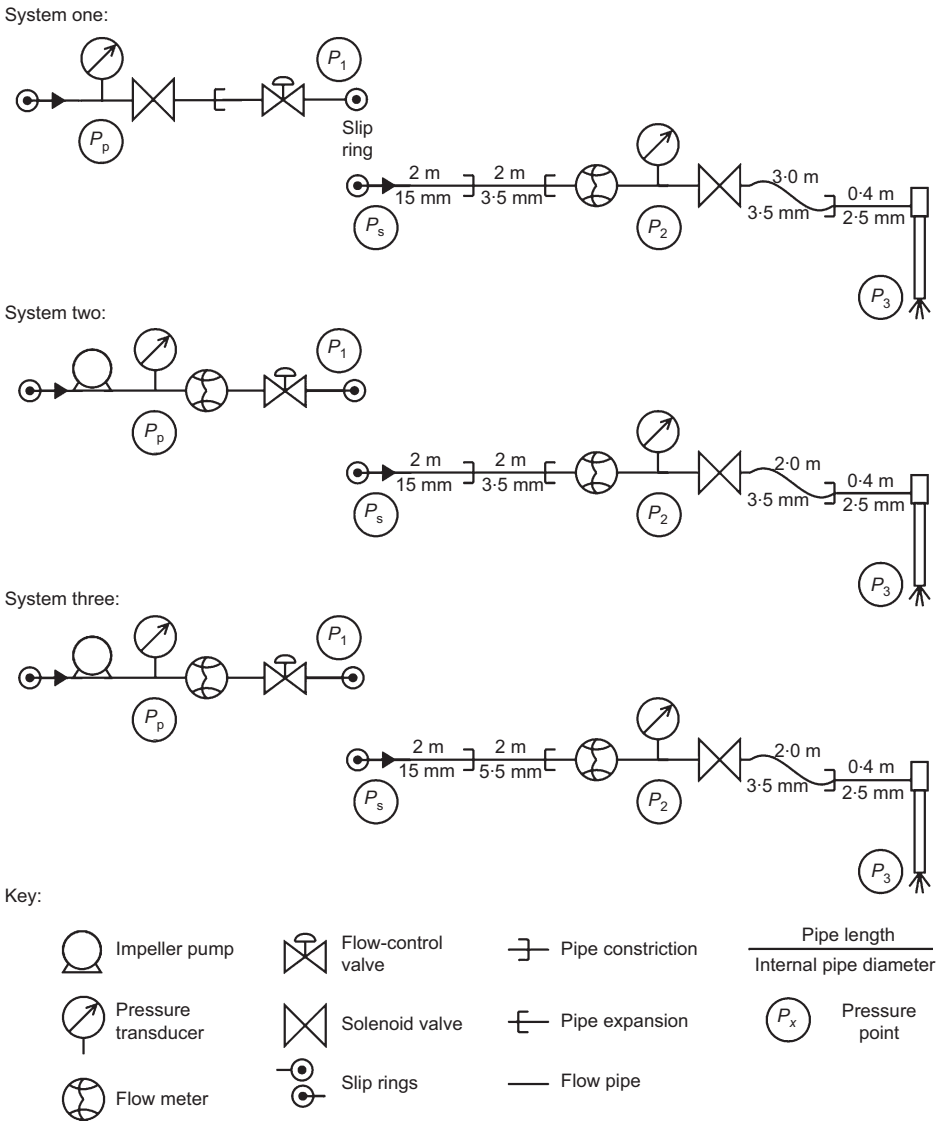

Figure 1. Hydraulic diagrams of the different systems used during testing

analytically, the case for a pipe expansion. For a flow moving from a pipe diameter D_1 to a larger pipe of diameter D_2, the loss factor is found using Equation 3

$$3. \quad k_{\text{expansion}} = \left(1 - \frac{D_1^2}{D_2^2}\right)^2$$

Other loss factors, for objects such as valves, are given by the manufacturer after their testing of the apparatus at different flow rates and pressures. Other, more common fittings, such as pipe contractions, can be assessed using similar expressions to Equation 3 for the pipe expansion, but determined experimentally, rather than by analytical methods (White, 1998).

For pipe losses, the value of λ is set by the Reynolds number of the pipe flow, $\text{Re} = (\rho VD)/\mu$ and the ratio of pipe roughness, k_s, in metres, to pipe diameter (Colebrook, 1938). The fluid velocity, V, is given in metres per second, and fluid viscosity, μ, in kilograms per metre per second. The value for λ is given by

$$4. \quad \frac{1}{\sqrt{\lambda}} = -2\log_{10}\left(\frac{k_S}{3{\cdot}7D} + \frac{2{\cdot}51}{\text{Re}\sqrt{\lambda}}\right)$$

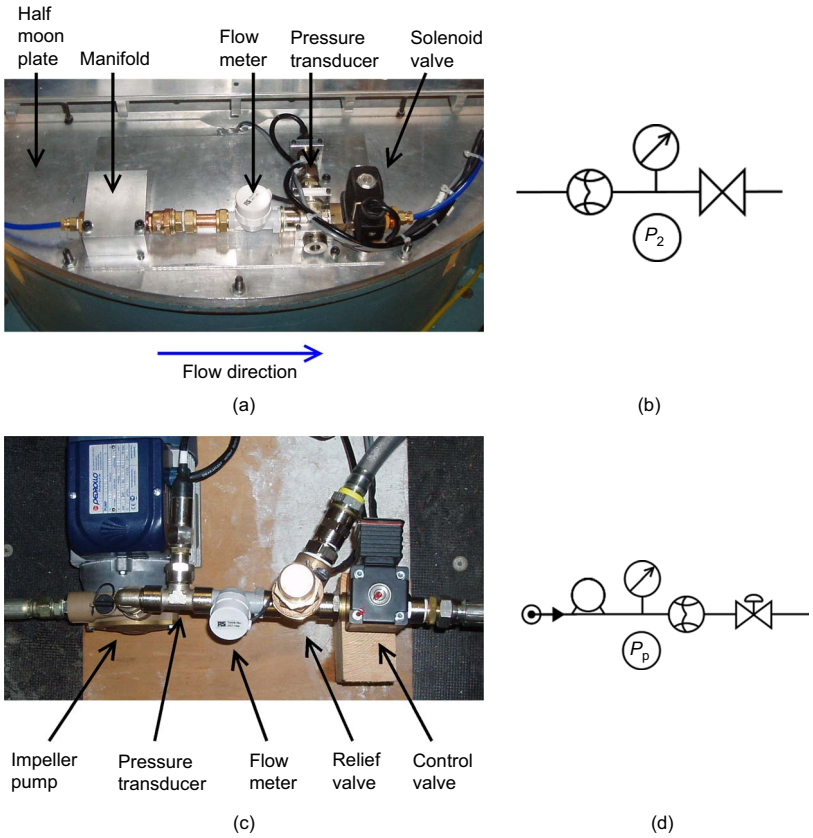

Figure 2. Details of the apparatus used to monitor flow conditions: (a) high pressure line on the package; (b) high pressure line schematic diagram; (c) impeller pump system before the slip rings; (d) impeller pump schematic diagram

Ultimately, Equation 2 demonstrates the link between the energy loss over a length of pipe and the flow rate. But Equation 4 highlights the dependency of λ on flow rate, which complicates the simple linear relationship proposed in Equation 1. However, an appropriate factor, which is constant with flow rate, can be found that minimises the error in the energy loss for a length of pipe.

In summary these formulae were used as far as possible to calculate the overall losses expected in the water injection experiments. For more complicated obstructions, however, the loss factor was derived from the experimental results instead.

4.2 Acceleration contribution

In addition to the pressure losses experienced throughout the system, the contribution from radial acceleration down the beam arm had to be found. The pressure at the package, P_2, is calculated by integrating the enhanced self-weight of the column of water along the beam arm from radius r_1 to r_2

$$5. \quad P_2 = \int_{r_1}^{r_2} \omega^2 r \rho \mathrm{d}r = \frac{\rho\omega^2}{2}(r_2^2 - r_1^2)$$

where ω is the radial acceleration of the beam in radians per second; and r is the radial distance from the beam centre in metres.

Combining these factors allows the pressure to be found at any point in the system. The relationship is based on Bernoulli's equation between two points along a streamline, as shown for a centrifuge by Goforth *et al.* (1991), but adapted for assessing the energy per unit volume, E, of the flow.

$$6. \quad P_1 + \frac{V_1^2\rho}{2} - \frac{\omega^2 r_1^2 \rho}{2} = P_2 + \frac{V_2^2\rho}{2} - \frac{\omega^2 r_2^2 \rho}{2} + \Delta E$$

4.3 Validation of pressure loss equations

Two steps were taken to validate the pressure calculation shown in Equation 6. The first was to find the pressure increase under different radial accelerations, and the second was to validate the linear relationship between energy loss and the flow rate squared.

4.3.1 Pressure increase along the beam arm

The pressure increase at zero flow rate was used to verify the contribution from radial acceleration, calculated using Equation 5. Zero flow was provided by closing the solenoid valve on the high pressure line, but leaving all other valves fully open. This ensured that the energy loss between points P_p and P_2 was $\Delta E = 0$, so that only the acceleration contribution remained. With this, Equation 6 simplifies to

$$7. \quad P_2 = P_p - \frac{\rho\omega^2}{2}\left(r_2^2 - r_p^2\right)$$

Experimental data for this stagnant condition are plotted against the values found from Equation 7. The results are shown in Figure 3 where the dashed line represents equality of the measured and calculated values. A slight difference is observed between the data points and the line of equality, mainly for system one. This difference is attributed to the variation in the supplied pressure, P_p, from the mains water supply. The result confirms the calculation for increasing pressure moving through the acceleration field.

4.3.2 Energy loss approach between points P_2 and P_3

Equation 6 was tested to confirm that the energy loss approach is appropriate for finding the pressure at the nozzle. The approach was tested for cases where the pile was suspended above the model surface, so that the pressure was known at both locations. With the pile in this position, a flow check was completed and the nozzle pressure was assumed to be atmospheric. In addition to investigating the energy loss in the pipe system, there would be a minor pressure increase owing to increased radius from the centrifuge centreline to the nozzle, compared to the measurement location.

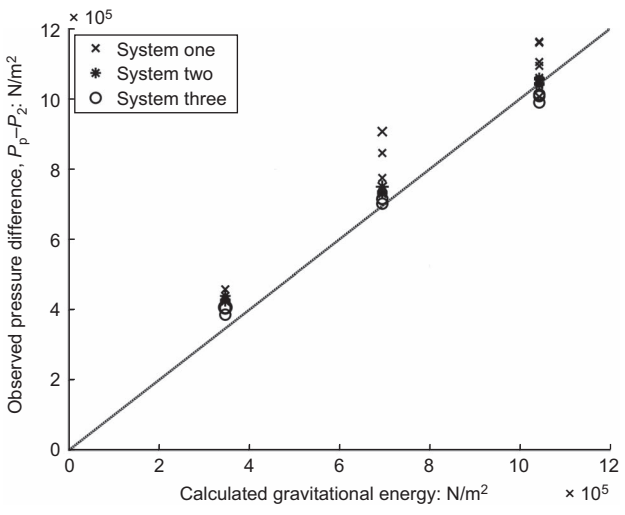

Figure 3. Comparison of the pressure increase contribution of the experiment and the calculation

A wide range of flow rates were tested, using various control valve positions. This allowed the expected linear relationship between the energy loss and flow rate squared to be investigated. For a successful flow check, stable flow conditions through the system had to be established. The average flow check lasted between 20–30 s, with each flow check forming a single data point. Flow checks were completed for various radial accelerations, 1g, 20g, 40g and 60g at the model base. Multiple flow rates were trialled at each radial acceleration.

In addition to the three systems trialled, different nozzles were tested. Three nozzles will be considered in this paper. All nozzles used were central orifice plate nozzles, 1·0 mm, 2·5 mm and 3·0 mm in diameter. These nozzles offered different termination modes for the flow exiting at the pile toe. The latter two had similar diameters to the delivery pipe, and generated a minor additional exit loss. On the other hand, the 1·0 mm nozzle attracted a significant loss, owing to the nozzle constricting the flow through the pile. The difference in nozzle geometry was observed to have a large effect on the loss factor for this system section.

A comparison must be made, between the experimental data and the calculated values, in order to validate the proposed energy loss approach. First, the experimental data will be plotted. Figure 4 shows the energy difference, ΔE, plotted against flow rate squared for the three systems and the three orifice nozzles. The energy difference was found by rearranging Equation 6 as

$$8. \quad \Delta E = P_1 - P_2 + \frac{\rho Q^2}{2}\left(\frac{1}{A_1^2} - \frac{1}{A_2^2}\right) - \frac{\rho\omega^2}{2}\left(r_1^2 - r_2^2\right) = a \times Q$$

For each individual system and nozzle combination, a dotted line of best fit is plotted for the data set, passing through the origin as there can be no energy loss at zero flow. All lines plotted have a linear regression, R^2, value greater than 0·90, indicating a good fit of the data to the proposed linear regression. Table 1 shows all the loss factors derived from the experiment results using different system and nozzle combinations.

The smallest, 1·0 mm diameter, nozzle attracts a disproportionately large loss – to the extent that the comparative effect of

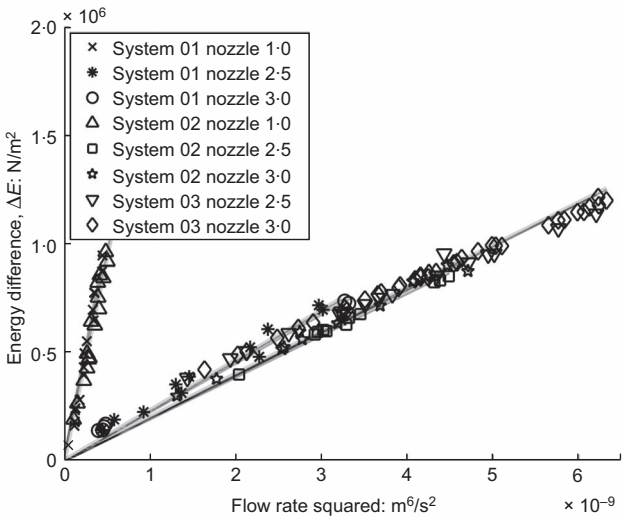

Figure 4. Assessment of the energy loss between points P_2 and P_3 for different system and nozzle configurations

the rest of the system is negligible. The two larger nozzles show the same loss factor, owing to the similarity between the nozzle and pipe diameters. The different systems also have some effect. This was a result of changing some of the pipes for wider bore pipes in order to increase the maximum flow rate.

To calculate the energy loss between points P_2 and P_3, there are five individual losses to consider: at the solenoid valve, two pipe lengths, a pipe constriction and an exit loss. Figures 5(a)–(e) shows the calculated loss factor for each individual loss, and demonstrates how the pipe losses dominate the total system loss. The figure also highlights how the smallest nozzle attracted a significant loss in comparison to the other losses in the system.

The individual loss factors are summed to find the total loss factor. This is shown in Figure 5(f) and the value is included in Table 1. A broad agreement is apparent between the calculation and the experimental results, with differences in system and nozzle performance included in the calculations. It is important to note that the loss factors are independent of the gravitational acceleration.

4.4 Calculation of pressure between points P_p and P_2

With the energy loss equation validated, attention can be turned to understanding the system between the pump, P_p, and the high pressure line, P_2, by way of the slip rings.

The same flow check data as earlier can be used to investigate the energy difference between the pump and the high pressure line. This includes the two most uncertain losses: across the flow-control valve and across the slip rings. Comparisons will be made using systems two and three, as both logged pressure and flow rate data at the pump in addition to the high pressure line. Again, data will be taken from a variety of flow rates and radial accelerations.

Working from the high pressure line first, the pressure immediately after the slip rings, P_s, can be found using Equation 6. The losses in the pipe work on the beam are well defined using the established relationships, and any error in the energy difference would be small. However, the calculations predicted large negative pressures after the slip rings, reaching $P_s = -400$ kPa. This is significantly lower than the cavitation pressure of water, and cannot be sustained in the saturated system as presented.

Reaching the same location, but from the impeller pump, it is unclear how the negative pressure arises. A large energy drop is achievable over the control valve, especially if the valve is heavily restricting the flow, and additional energy will be lost

System	Nozzle diameter: mm	Experimental loss factor: Ns^2/m^8 ($\times 10^{14}$)	R^2	Calculated loss factor: Ns^2/m^8 ($\times 10^{14}$)
1	1·0	20·26	0·97	16·68
1	2·5	2·31	0·94	2·35
1	3·0	2·26	0·98	2·34
2	1·0	18·84	0·97	16·01
2	2·5	1·93	0·99	1·90
2	3·0	2·00	0·97	1·90
3	2·5	1·98	0·92	1·90
3	3·0	1·98	0·96	1·90

Table 1. Comparison of measured and calculated loss factors for the different system and nozzle combinations

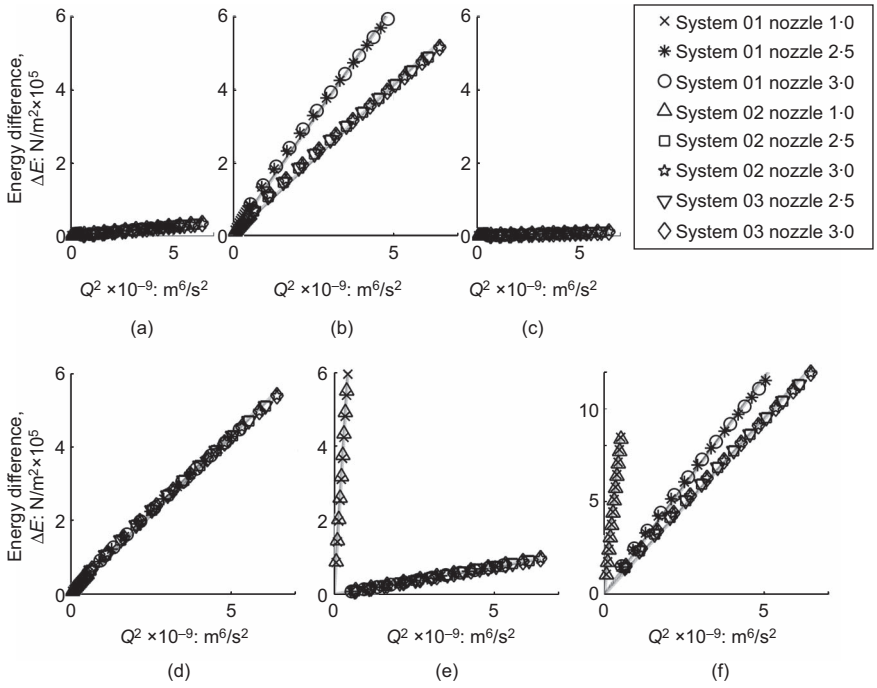

Figure 5. Calculated loss factor for each individual component between P_2 and P_3: (a) valve; (b) 3·5 mm; (c) constriction; (d) 2·5 mm pipe; (e) exit; (f) summed loss

over the slip rings. However, there is no reason for the pressure to be falling to such a large negative pressure.

Instead, the pressure at the slip rings will be assumed to be atmospheric, or slightly below. For this assumption to be valid, a point for air to enter the pipework is required. A low pressure in the slip rings would be sufficient to draw air into the pipework, and as a result the system would become partially saturated. This was corroborated by the visual confirmation of bubbles in the pipework, which appeared to move through the manual flow-control tap of system one in the opposite direction to the flow at restricted flow rates.

The introduction of air into the system invalidates the previous assumption of a fully saturated system. This occurs when the flow being provided to the pile is restricted, so that head losses reduce and an unsustainable partial vacuum is induced at the fluid slip rings. Instead, atmospheric air is drawn in, and this section of pipework simply delivers a trickle of water at atmospheric pressure to the phreatic water surface at r_w. This surface marks the beginning of the saturated water column, that provides pressure to the high pressure line and the pile. An illustration of the partially saturated system is shown in Figure 6.

Using the flow rate and pressure data logged at the high pressure line, the position of the phreatic surface, r_w, can be inferred using Equation 6. This assumes the air filled gap is at atmospheric pressure. Figure 7 shows the deduced phreatic surface position for the partially saturated system, plotted against the calculated pressure at the slip rings, on the assumption that the system remained saturated. When the pressure at the slip rings falls negative, the calculation corrects for this and allows for an air gap to form. The figure does not show the gradually reducing flow rate with reducing water column height.

It was important to show that this effect was the inevitable result of restricting the water supply, and not simply low flow rates experienced owing to a deep installation. Additional data from model piles installations were used, where the supply remained unrestricted throughout the installation. The flow rate reduced at large flow rates, owing to the interaction of the surrounding sand body with the pile. These data were used to calculate the pressure at the slip rings, which was found never to fall negative during such low flow periods. This result confirmed that the calculated negative pressure was actually attributable to air entering the system as a result of limiting the water supply to the centrifuge, rather than the low flow rate itself.

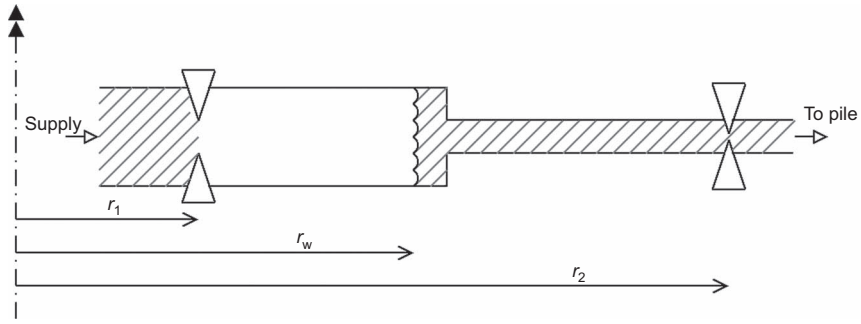

Figure 6. Illustration of a partially saturated system

4.5 Calculation of the nozzle pressure, P_3, during a pile installation

With the validation steps complete, the nozzle pressure at the pile toe, P_3, can confidently be calculated for all conditions. It was important to know the nozzle pressure, in order to understand the geotechnical mechanism governing water injection.

Using the energy loss equation, Equation 6, the nozzle pressure could be predicted based on any monitored pressure in the system. This could be either the pressure logged at the pump or at the high pressure line. Combined with the measured flow rate and loss factor of the system, a robust method for finding the nozzle pressure was available. Clearly, uncertainties are reduced by minimising the distance, and therefore the losses, between the measurement location and the point of interest, but any position can be used. For the case of the pile installations, only the high pressure line data were used to find the nozzle pressure.

5. Installation results

The purpose of developing the new water supply was to investigate the effects of water injection-aided pile installations. Water injection is considered a useful method for reducing pile resistance during installation. However, little work has previously been completed on examining the mechanisms governing this load reduction, or the effects of the process on the final pile performance and surrounding ground conditions. Work was completed, installing model piles using various injection conditions, to investigate the different effects on pile installation.

Figure 8 shows an example of the calculation applied to a complete installation, plotted at model scale. All the installations were completed with an acceleration of 60***g*** at the base of the model. Each pile was installed at a rate of 1·0 mm/s to a

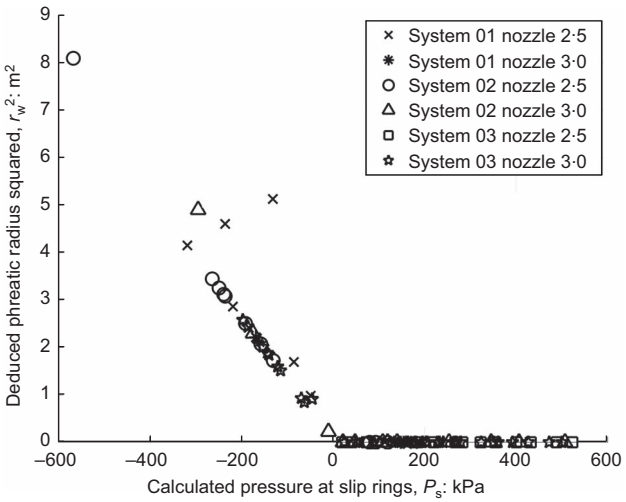

Figure 7. Deduced phreatic radius r_w for different flow rates and systems

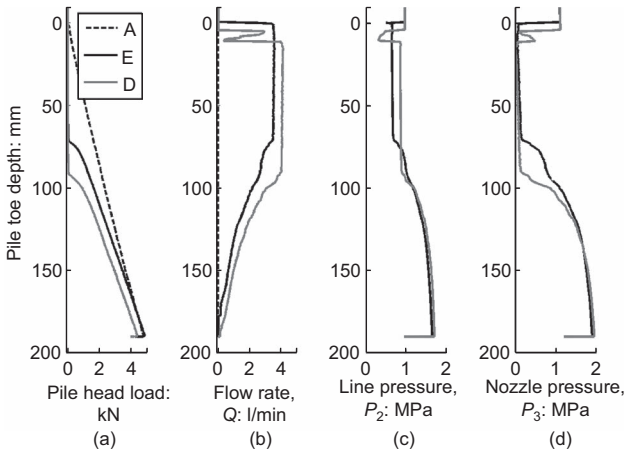

Figure 8. Three installations using the 3·0 mm diameter orifice nozzle

depth of 190 mm and used the 3·0 mm orifice nozzle and water supply system two. Of the three installations shown, A was completed without supplementary water injection, whereas D and E both used water injection, but at different maximum flow rates.

Figure 8(a) shows the pile head loads against the depth of installation, monitored using strain gauges. Figure 8(b) and 8(c) show data of flow rate and pressure respectively, logged at the high pressure line during the installations. These two figures can be used, with Equation 6, to find the nozzle pressure, which is plotted in Figure 8(d). The calculation allows for the changing nozzle position in the acceleration field.

The effect of supplementary water injection eliminates pile resistance during the initial stage of pile installation. At this point, the injected flow rate is the same as the maximum achievable flow rate from the system. After the first stage of installation, the flow rate begins to be throttled off, by the response of the sand around the pile base. As the flow rate reduces, the energy loss between the high pressure line and the nozzle also reduces, and so the nozzle pressure increases.

This effect appears counter-intuitive, with the injected flow rate reducing despite an increasing nozzle pressure driving the flow through the sand. However, during pile installation, crushing of particles at the pile toe forms a region of low permeability around the injection nozzle, which in turn limits the achievable flow rate through the sand body. With increasing depth, and increasing pile load, more particle crushing takes place. This exacerbates the reduction in permeability, until an almost impermeable plug of very crushed particles exists at the injection nozzle and any noticeable flow is prevented, despite 2 MPa nozzle pressure.

6. Maintaining centrifuge balance

It was essential to control the mass inbalance owing to the build-up of water throughout a centrifuge test. The Turner beam centrifuge has a fixed mass counterweight, and therefore the experiment mass should ideally also remain unchanged. The maximum allowable difference in mass between the counterweight and the experiment is 10 kg at 100$\boldsymbol{g}$ acceleration, and this only for short periods.

To achieve a constant experiment mass, any water added during injection should be expelled using the standpipe system. The response was logged during testing, by monitoring the water pressure at the standpipe base. These measurements could be used to ensure that water was draining from the standpipe, out of the model and into the centrifuge chamber. The model layout and transducer locations is shown in Figure 9. The sand body is connected to the base of the standpipe, and any excess water flows out of fixed drainage holes at the top.

During a flow check event, the standpipe water level should remain constant. The water level in the model may rise slightly, forming a pressure gradient sufficient to drive flow into the standpipe. Instruments in the model body were relied upon to ensure the water level remained within the limits, whilst an instrument at the standpipe base was used to monitor the correct functioning of the standpipe.

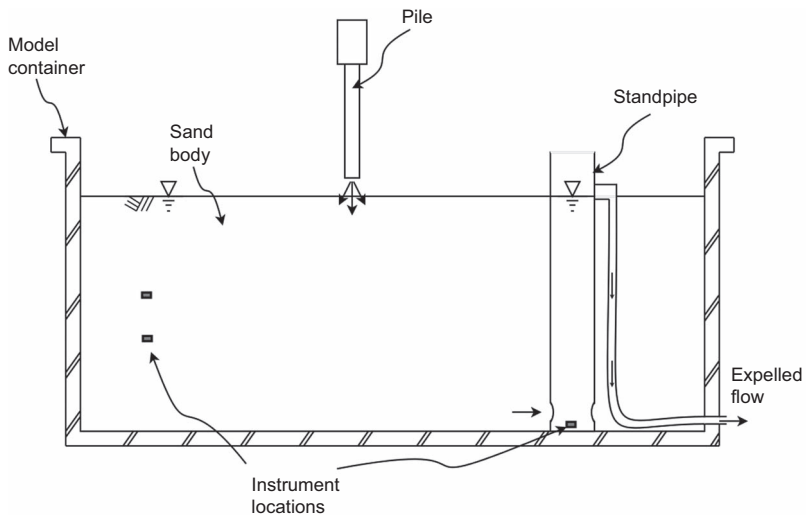

Figure 9. Standpipe and transducer cross-section

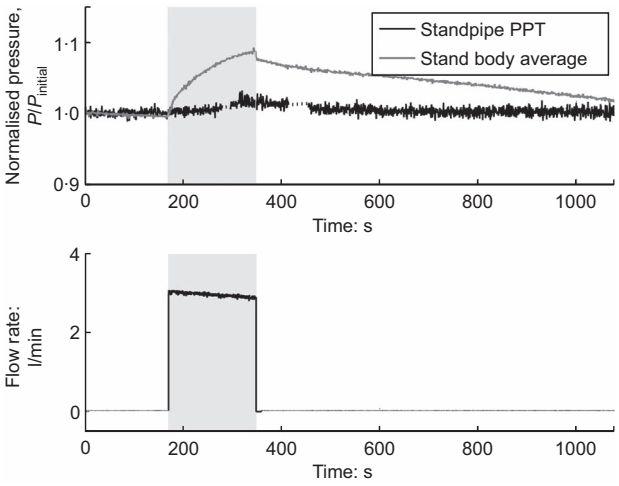

Figure 10. Changes in the model water table during a water injection event

Figure 10(a) shows the average response of pore pressure transducers in the model and stand pipe during a flow check procedure, where water was injected directly onto the sand surface. The dotted sections of the stand pipe reading indicate brief periods where the instrument failed. Information on the injected flow rate is plotted in Figure 10(b).

A total of 9 l of water was added to the model during the flow check. This corresponded to an increase of 16 mm in the water table level, giving 10 kPa at the model pressure transducers at 60***g*** acceleration. At the level of transducers in the sand body, such a water table increase would result in a normalised pressure of 1·08, where the normalised pressure is the pressure monitored by the instrument divided by the initial reading before water injection.

Figure 10 shows a significant increase in the water table in the sand body, but only a small increase in the standpipe water level. This met the expected operating conditions of the standpipe. The rise in the average normalised pressure in the model was continually monitored using the data logging software, declared to the technician who was responsible for safety. A normalised limit pressure of 1·1 was imposed, such that if the normalised pressure exceeded this value, then injection would be immediately terminated and the model allowed time to drain back to its initial conditions. The standpipe measurement was also carefully tracked, to ensure that the model was able to drain sufficiently throughout the test.

The lag observed in the normalised pressure of the model highlights the problems of injecting large flow rates into a centrifuge model, and how difficult they are to immediately expel. The position of the standpipe meant that a pressure gradient was required for fluid to flow into the standpipe base, but it was possible to reach equilibrium, injecting 3 l/min into the model and achieving sufficient drainage, without exceeding the normalised limit pressure. When using systems two and three, where larger flow rates were injected, a second standpipe was provided to increase the drainage capacity of the model.

7. Conclusions

In conclusion, a new water supply system was successfully commissioned for the supply of high pressure water at large flow rates for use on the geotechnical beam centrifuge at University of Cambridge. The system was capable of delivering peak flow rates of 6·0 l/min, and peak pressures of 2 MPa at the experiment package. It was demonstrated that a well-monitored standpipe system was sufficient to ensure the model was in balance throughout testing.

An energy balance approach was presented, to account for pressure losses in a pipe network and potential energy gain under centrifugal acceleration. The energy approach enables water pressures to be estimated at positions remote to the measurement location. The approach was validated against a series of data sets and calculated predictions. A technique has been demonstrated that allows for atmospheric air to be drawn into the delivery line at the fluid slip rings.

Finally, a high-quality data set was formed, which allowed the pressure at an injection nozzle to be continuously calculated during a pile installation. Knowledge of this nozzle pressure proved valuable for the assessment of the mechanism governing water injection-aided pile installations.

REFERENCES

Colebrook C (1938) Turbulent flow in pipes, with particular reference to the transition region between smooth and rough pipe laws. *Journal of the Institution of Civil Engineers (London)* **11**: 133–159.

Gaudin C, Bienen B and Cassidy M (2011) Investigation of the potential of bottom water jetting to ease spudcan extraction in soft clay. *Géotechnique* **61(12)**: 1043–1054.

Goforth G, Townsend F and Bloomquist D (1991) Saturated and unsaturated fluid flow in a centrifuge. *Proceedings of Centrifuge '91* (Ko HY and McLean FG (eds)). A.A. Balkema, Rotterdam, The Netherlands, pp. 497–502.

Ko HY (1988) Summary of the state-of-the-art in centrifuge model testing. *Centrifuges in Soil Mechanics* (Craig WH, James RG and Schofield AN (eds)). A.A. Balkema, Rotterdam, The Netherlands, pp. 11–18.

Schneider JA, Lehane BM and Gaudin C (2008) Centrifuge

examination of pile jetting in sand. In *Press-in Engineering 2009 – Proceedings of 2nd IPA International Workshop, New Orleans*. International Press-in Association, Tokyo, Japan, pp. 17–24.

Schofield AN (1980) Cambridge geotechnical centrifuge operations. *Géotechnique* **30(3)**: 227–268.

Taylor R (ed.) (1995) *Geotechnical Centrifuge Technology*. Blackie Academic & Professional, London, UK.

Tomlinson M and Woodward J (eds) (2008) *Pile Design and Construction*. Taylor & Francis, London, UK.

White FM (ed.) (1998) *Fluid Mechanics*. McGraw Hill, New York, NY, USA.